Journal of Flow Visualization and Image Processing, vol. 2, pp. 299–310, 1995 Copyright © 1995 by Begell House, Inc.

TOMOGRAPHIC DECONVOLUTION OF LASER SPECKLE PHOTOGRAPHY FOR AXISYMMETRIC FLAME TEMPERATURE MEASUREMENT

T. E. Walsh and K. D. Kihm
Department of Mechanical Engineering, Texas A&M University, College Station, Texas 77843–3123

A laser speckle photography technique can nonintrusively measure thermal flow properties such as medium density, index of refraction or temperature. The laser specklegram records a line-of-sight or path-integrated information on these properties. For varying properties in a medium along the optical path, a mathematical technique called a tomography deconvolves cross-sectional information out of the projected measurement. The present work will outline the underlying principles of optical tomography and show how to apply it to the diagnostic technique of laser speckle photography. Comparisons of temperature measurements using a thermocouple probe against the temperature conversion from the specklegram data have been made for laminar flames. The speckle photography technique shows good potential as a new nonintrusive temperature measurement tool for various thermal flows.

INTRODUCTION

Much research has been devoted to the area of experimental thermal fluid mechanics to find basic thermodynamic properties of gaseous media. Making the interrogation technique nonintrusive for high accuracy measurements is desirable. These requirements demand the need for dependable optical measurement devices. In past decades, laser interferometry has been the primary technique for nonintrusively determining two- and three-dimensional temperature and density fields. Laser speckle photography, a relatively new laser-optical method, is gaining acceptance rapidly as an improvement over interferometry.

Although it shares many of the same light refraction principles as interferometry, laser speckle photography has a higher signal density, greater ease of use, and lower experimental cost than interferometry [1]. The foremost advantage of the specklegram technique is its excellent spatial resolution. Where an interferometer has a limited accuracy dictated by the number of fringes present in an interferogram and the ability to count the number of fringe shifts, the specklegram's accuracy is limited in principle by the resolution of laser speckles on the photographic plate, which could be as small as a few microns. This is important when 3-D temperature fields are reconstructed by way of optical tomography, where signal-dense projections are advantageous for higher accuracy in the conversion.

The present experimental study focuses on demonstrating techniques for expanding the laser specklegram method to reconstruct two-dimensional (cross-sectional) index of refraction fields from one-dimensional (line-of-sight) data sets. This is accomplished by a

strictly mathematical procedure called tomography. The interest recently focused on this field is primarily due to the success of medical imaging such as CT (computed tomography) scans that determine cross-sectional human tissue composition from hundreds of line-of-sight X-ray projections with different viewing angles. Many specific details concerning the broad field of tomography are credited to other publications [2,3,4], and only a brief review of pertinent discussions follows.

The laser specklegram technique [5] has been applied successfully to many two-dimensional heated flows where the thermal properties remain nearly unchanged along the optical path [1, 6, 7]. Furthermore, speckle photography can analyze spatially and temporally fluctuating flow fields that otherwise would be very difficult by interferometer [8]. When the test field cannot be approximated as infinite in the line-of-sight direction, a mathematical technique called tomography can determine two-dimensional index of refraction fields from one-dimensional, projected data sets. The test field for asymmetric situations must be interrogated from many different directions yielding many projections that must be simultaneously deconvoluted. Stacking up these two-dimensional conversions will construct a fully three-dimensional image from the projected two-dimensional information. Several mathematical techniques have been developed to carry out this process.

The two most popular methods for performing this transform involve either Fourier domain methods [9] or the algebraic solution to a nonunique system of equations, termed algebraic reconstruction technique (ART) [10]. When an experimental test field is axisymmetric, the mathematical deconvolution is greatly simplified, as only one projection is required. This reduced deconvolution from the Fourier domain method is called Abel conversion and used in the present study to optically evaluate an axisymmetric index of refraction distribution.

ABEL CONVERSION

Fermat's principle states that light rays seek the shortest path in a medium with distributed index of refraction. Consider laser light ray propagating in the x-direction incident on an axisymmetric index of refraction field, $n(x,y)$ in Figure 1. The mathematical expression of the Fermat's principle is [11]:

$$\frac{d}{ds}\left[n\frac{d\vec{r}}{ds}\right] = \vec{\nabla}n \tag{1}$$

where n represents the index of refraction of medium, s denotes the coordinate along the light ray, and $\vec{r}$ represents the position vector of an arbitrary point on the light ray. As light crosses through the test medium, it refracts continuously along the path. For small refraction angles ($ds \quad dx$, and $\xi_2 \approx \xi_2'$) with a paraxial approximation where the light rays are assumed to remain in the x-y plane, Equation 1 is reduced to:

$$\frac{\partial}{\partial x}\left[n\frac{\partial y}{\partial x}\right] = \frac{\partial n}{\partial y} \tag{2}$$

Integrating both sides of Equation 2 from ξ_1 to ξ_2 gives:

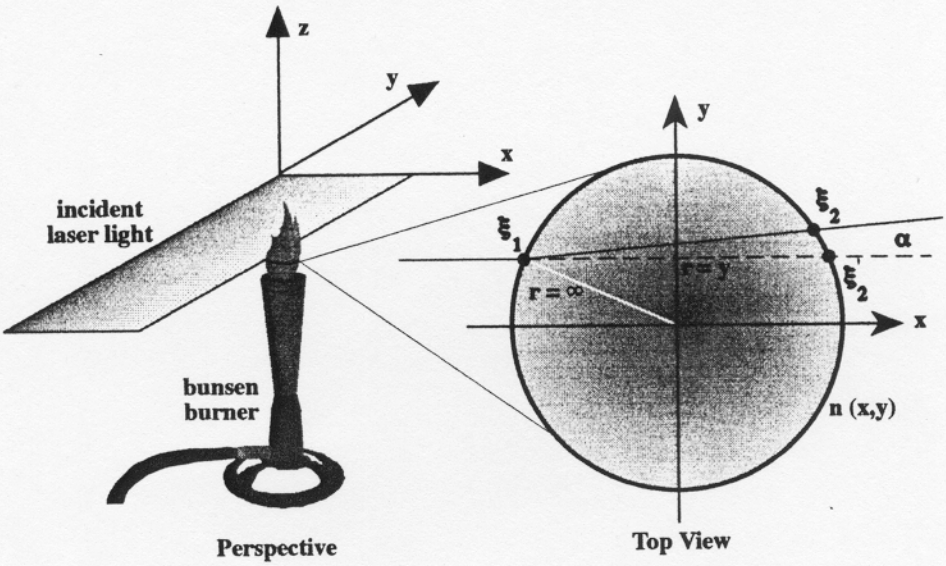

Fig. 1 Axisymmetric domain with line-of-sight laser light projection.

$$\left[n\frac{dy}{dx}\right]_{\xi_1}^{\xi_2} = 2\int_0^{\xi_2}\frac{\partial n}{\partial y}dx$$

$$n_0\alpha(y) = 2\int_0^{\xi_2}\frac{\partial n}{\partial y}dx \tag{3}$$

where the slope of a light ray, dy/dx is zero at the entrance of the test medium and is equal to $\alpha(y)$ at the exit with dy/dx being an infinitesimal amount. The index of refraction is recovered to the ambient value, n_0 at both the entrance and exit.

Transforming Equation 3 into polar coordinates can be done with a coordinate transformation:

$$r^2 = x^2 + y^2; \quad \frac{\partial r}{\partial y} = \frac{y}{r}; \quad \frac{\partial r}{\partial x} = \frac{x}{r}; \quad dx = \frac{\partial x}{\partial r}dr$$

$$n_0\alpha(y) = 2\int_0^{\xi_2}\frac{\partial n}{\partial r}\frac{\partial r}{\partial y}dx = 2\int_0^{\xi_2}\frac{\partial n}{\partial r}\frac{\partial r}{\partial y}\frac{\partial x}{\partial r}dr$$

$$= 2\int_y^{\infty}\frac{\partial n}{\partial r}\frac{y}{r}\frac{r}{x}dr = 2y\int_y^{\infty}\frac{\partial n}{\partial r}\frac{dr}{\sqrt{r^2 - y^2}} \tag{4}$$

$$\boxed{\alpha(y) = 2y\int_y^{\infty}\frac{\partial}{\partial r}\left[\frac{n}{n_0}\right]\frac{dr}{\sqrt{r^2 - y^2}}}$$

Equation 4 is termed projection function or *Forward Transform*. Measurement of laser speckle dislocations provides the projection function, $\alpha(y)$, which represents a path-integral of the index of refraction variation in the test medium. True radial distribution of the index of refraction, $n(r)$, must be determined from the projected angular refraction $\alpha(y)$. Fortunately, Equation 4 represents an integral transform of the Abel type. The *Inverse (Abel) Transform* of Equation 4 is given as [4]:

$$\frac{n(r)}{n_0} = 1 - \frac{1}{\pi}\int_r^\infty \frac{\alpha(y)}{\sqrt{y^2 - r^2}}\,dy \tag{5}$$

Discrete values of $\alpha(y)$ obtained from a laser speckle photograph are interpolated with piecewise polynomial functions that allow for numerical integration of Equation 5 for calculating $n(r)$.

SPECKLE PHOTOGRAPHY

A previous publication [12] gives a detailed description of the present laser speckle photography system. Therefore, only a basic explanation will be provided of the method. When coherent and collimated light rays of an expanded laser beam diffract from the granular surface of a ground glass plate (Figure 2), the random interference of rays will construct three-dimensional distributions of random patterns of coherent (bright speckles) or incoherent (dark speckles) interferences. With a test section in place, the local change in the index of refraction steers light rays to refract and by that dislocates the speckle locations about their original locations without the test section. Thus, a double-exposed photograph of both instances will yield a photographic negative, called a specklegram, of the entire test field represented by thousands of randomly shaped diffraction gratings or optical speckles.

When a secondary laser illuminates the photographic negative, the average dislocations of those speckle pairs within the beam cross-section create a series of Young's fringes. The fringe spacing is measured to find the projected diffraction angle α. The measurement is repeated with the beam location varied to provide the projection function $\alpha(y)$. The data resolution can now be reduced as small as the beam diameter. From the geometrical optics consideration, the fringe spacing is given by [12]:

$$s = \frac{\lambda d}{\Delta} \tag{6}$$

where s is the fringe spacing, λ denotes the wave length (presently 632.8 nm of He-Ne laser), d represents a geometrical constant, and Δ is the dislocated speckle distance. Incorporating other system parameters, Equation 6 can be converted into an expression for the projection function $\alpha(y)$ as:

$$\alpha(y) = \frac{1}{s(y)}\frac{\lambda d}{c}\frac{m}{m'} \tag{7}$$

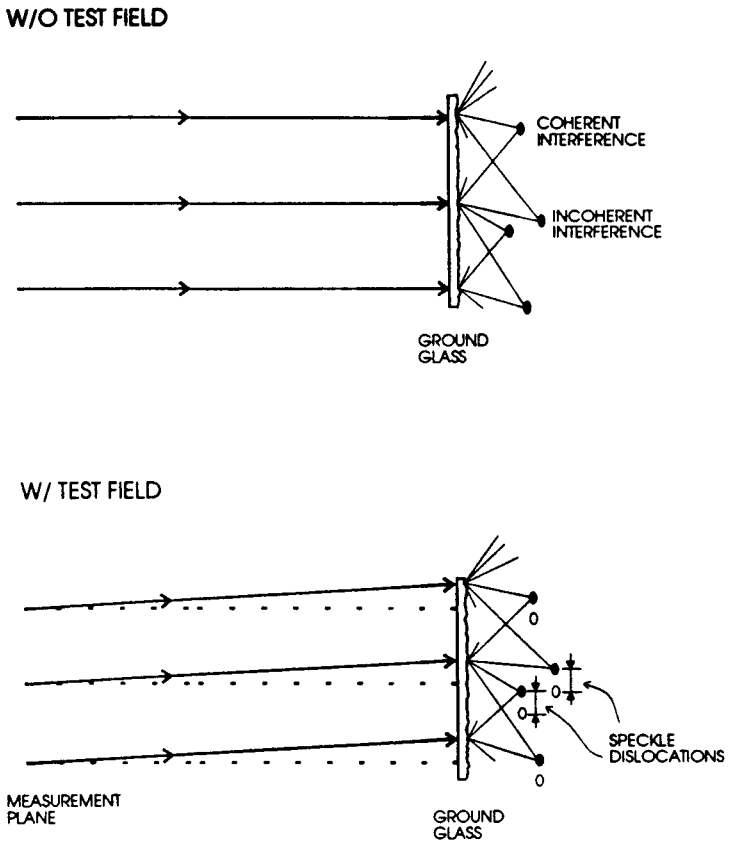

Fig. 2 Schematic illustration of formation of optical speckles and their dislocations.

where the constants c, m, and m' are parameters from the optical configuration of the speckle photography system. Note that α is inversely proportional to s, which dictates that narrowly spaced fringes represent a large angular refraction of light and thus a larger local temperature gradient.

The speckle photography system is essentially comprised of a beam expansion, collimation through a test section, speckle formation off the ground glass, and construction of double-exposed speckle images (Figure 3). The present specklegram system has two 318-mm-diameter parabolic mirrors of 1911 and 2553 mm focal lengths, respectively. The distance between the ground glass and the speckle plane is the defocusing length. Maintaining a minimal defocusing length is necessary, yet must be distinctive enough for recording speckle dislocations. A defocusing distance of 25 mm was optimal for the present measurements.

RESULTS AND DISCUSSIONS

Results are presented for a pure diffusion type flame of a paraffin candle and for a premixed type propane flame from a Bunsen burner. For the Bunsen flame, an attempt has

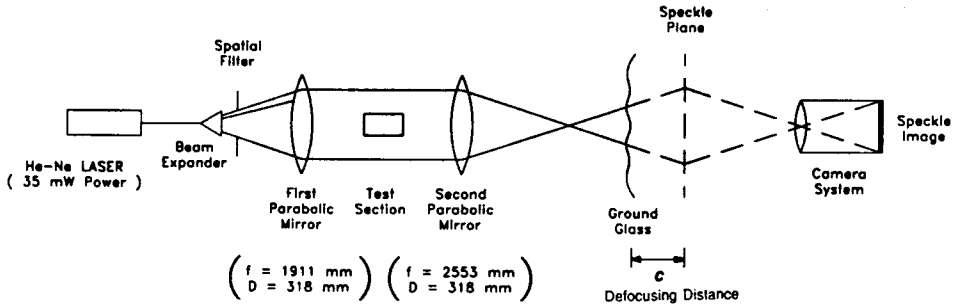

Fig. 3 A schematic description of laser speckle photography system.

been made to compare temperature data based on the speckle dislocation measurement against the thermocouple-measured data. The candle flame did not allow any reliable temperature data as the thermocouple probe interferes with the diffusion flame severely and renders the flame unstable.

Paraffin Candle Flame

Figure 4 presents Young's fringe patterns constructed at different axial (z) and transverse (y) locations on a specklegram taken for a diffusive candle flame. A narrower fringe pattern represents a larger refraction angle resulting from a higher temperature gradient and vice versa for fringes with wider spacing. Along the centerline a zero temperature gradient of symmetry condition provides no speckle dislocation and an infinite fringe spacing is detected. The temperature gradient becomes zero at larger r as the undisturbed ambient condition is approached. The fringes form perpendicular to the temperature gradient showing the primary direction of heat transfer. The paraxial condition, which assumes all the ray refractions remain in the same x-y cross-sectional plane, requires temperature gradient to exist only in the radial direction and all the fringes to orient in the z-direction. This condition is well satisfied in the middle ($z = 20$ mm) of the flame, whereas the distorted fringe orientations near the wick ($z = 0$) or farther downstream ($z = 40$ mm) invalidate the paraxial assumption.

Equation 7 with measured fringe spacing values determines the (projected) angular refraction. Figure 5 shows the angular ray refraction when passing a diffusive candle flame as a function of y at $z = 20$ mm. The curve represents a combination of a linear interpolation near the center, piecewise polynomial in the middle, and an exponential decay near the flame edge. The peak of the curve corresponds to the location of minimal fringe spacing in Figure 4. Tomographic deconvolution now converts the projected or path-integrated angular refractions in Figure 5 to determine the refractive index distribution as a function of r.

Equation 5 calculates the index of refraction vs. r from the projected (or measured) angular refraction. The results are presented in Figure 6. The refractive index of a gas is given by the Gladstone-Dale relation [13], which is expressed under ideal gas assumption as:

$$n = 1 + K\rho = 1 + K\frac{p}{RT} \tag{8}$$

where K is the Gladstone-Dale constant (0.226×10^{-3} m^3/kg at $\lambda = 632.8$ nm of He-Ne laser through air), p (Pa) is the pressure, and R is the gas (flame) constant. The index of refraction decreases with increasing temperature. Thus, the lowest index of refraction at the center of the candle flame in Figure 6 corresponds to the highest centerline temperature.

Conversion of Refractive Index into Temperature

Applying the Gladstone-Dale equation (Equation 8) once for a reference point denoted by a subscript 0 and then for any arbitrary point, and then combining the two equations gives:

$$\frac{T(r)}{T_0} = \left[\left(\frac{n(r)}{n_0} - 1\right)\left(\frac{RT_0}{KP_0} + 1\right) + 1\right]^{-1} \tag{9}$$

where the properties at the reference point must be specified and the centerline at $r = 0$ selected as the reference point for the present data. Due to the extremely high sensitivity of temperature dependence on refractive index, certain foreseen challenges arise in converting the refractive index into the temperature profile in Equation 9. For example, the relative variation of a refractive index from ambient conditions of 300 K ($n = 1.000027$)

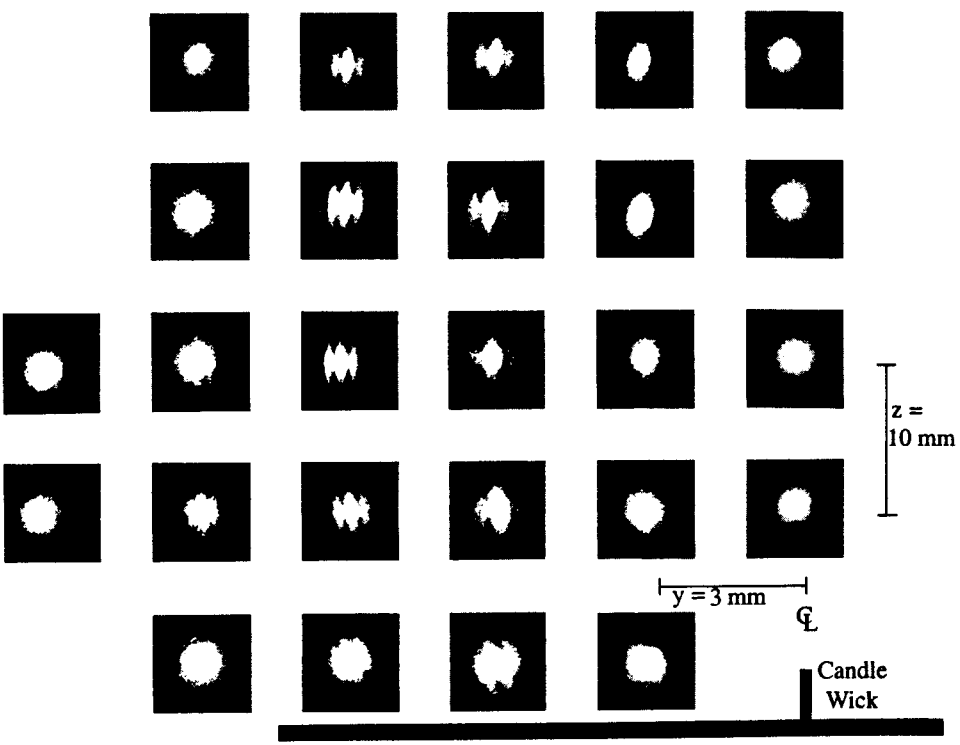

Fig. 4 Spatial distribution of Young's fringes generated from a laser specklegram recorded for an axisymmetric paraffin candle flame.

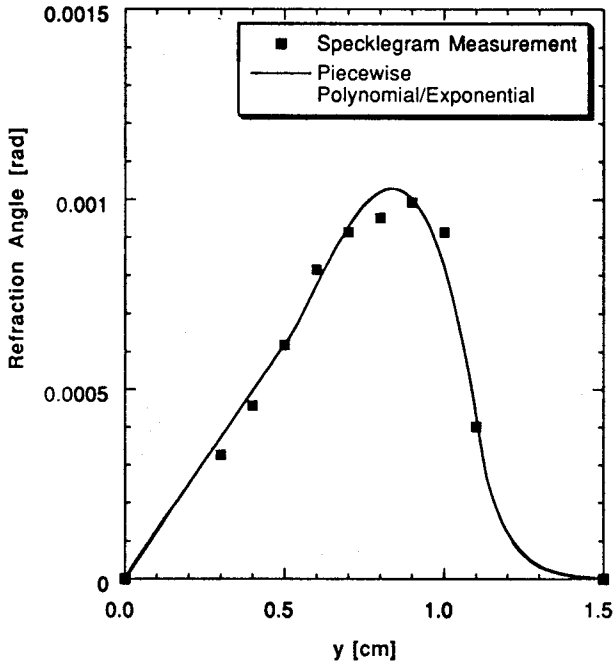

Fig. 5 Projected refraction angle directly measured from Young's fringes for an axisymmetric paraffin candle flame.

to 1300 K (n = 1.000006) is mere 0.002%. Examine the right-hand side of Equation 9 and note that not only does one need to perform a subtraction of two numbers extremely close to each other, but the resulting value is then multiplied by a number on the order of 10^3 to 10^4. This algebraic stiffness requires numerical calculations to be carried out to the tenth to twelfth decimal place to reduce numerical diffusion errors.

The second area of concern lies within the mathematical nature of the deconvolution of the index of refraction. Because the angular refraction and temperature gradient are directly proportional, to determine the temperature profile one must first deconvolve the temperature *gradient* profile from the angular refraction projection. The computation starts from a reference point of known temperature and continually integrates the computed gradient to determine the temperature at a location away from the reference point. However, this continuous integration of gradient information generally magnifies the error due to its accumulation. The farther one computes from the reference location, the larger accumulated error in temperature values results. Temperatures deconvoluted near the reference location have the potential to be highly accurate, while temperatures at the far end of the test field may be inaccurate.

Propane Bunsen Flame

Figure 7 shows the refraction angle determined from the fringe spacing measurement at z = 50.8 mm for a Bunsen propane flame. The piecewise polynomial function fitted for the refraction angle data is a linear interpolation near the flame center, a parabolic variation

around the peak, and an exponential decay near the flame edge. The speckle fringes did not always vertically orient and the flame had a nonzero temperature gradient in the flow direction. For some measurements, usually near the ambient edge of the test field, the fringes inclined as much as 30 degrees with the vertical, which evidences the ray refraction occurring away from the x-y plane. The optic theory evaluating the angular refraction is based on the assumptions of all the ray refractions occurring within the plane. The data shown in Fig. 7 represent a root-mean-square of the radial and vertical components of the overall angular refraction. These values would be overestimated for the temperature conversion under an assumption of radial-only refraction.

Accurate correction for the nonradial refraction would be very complicated because the local information on both the refraction direction and its magnitude must be considered. The tomographic deconvolution must be simultaneously carried out for these two measured data sets. Although not a rigorous solution, it can be hypothesized that a first approximation may be made of the radial correction by multiplying the measured angular refraction with the cosine of the fringe inclination with the vertical. That is, $\alpha_{radial}(y) \approx |\alpha| \cdot \cos\theta$, and

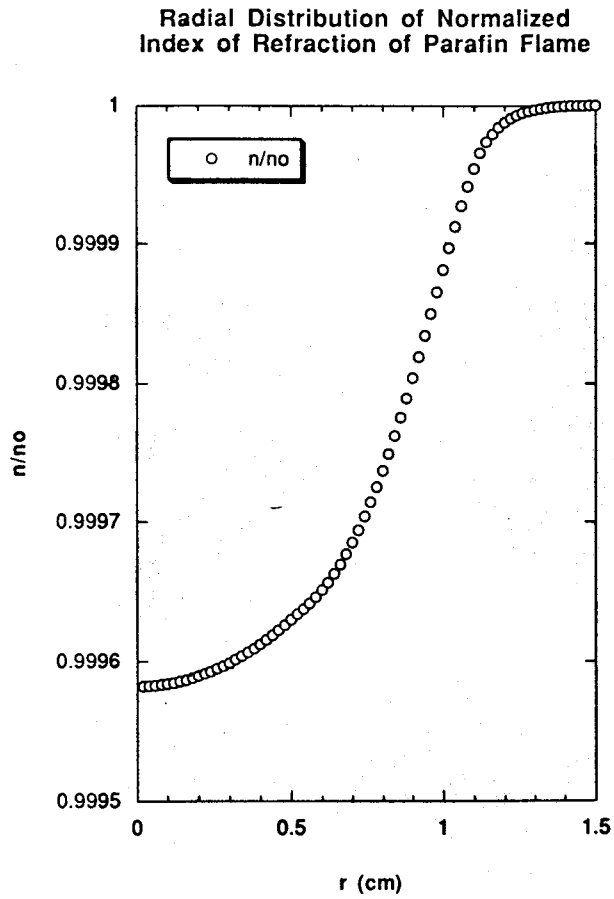

Fig. 6 Deconvolved radial distribution of refractive index of a paraffin candle flame.

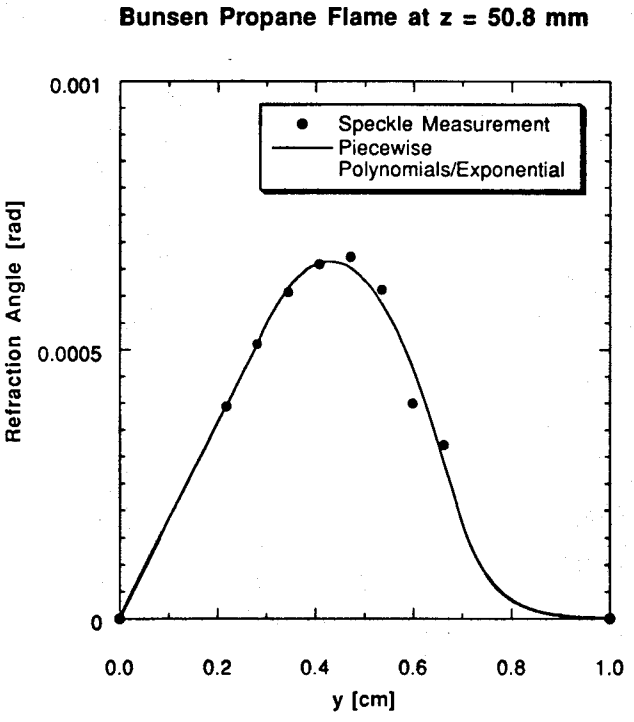

Fig. 7 Projected refraction angle directly measured from Young's fringes for an axisymmetric propane Bunsen flame.

such a simple correction would lower the overall magnitude of the $\alpha(y)$ distribution by as much as 20% for the present case. Consequently, this would affect the resulting temperature profile calculated from the Abel Transform of the specklegram data by as much as 15% at $r =$.

Figure 8 presents radial temperature distribution converted from the index of refraction using Equation 9. The symbols represent temperature data measured using an intrusive Platinum-Rhodium B-Type thermocouple probe. The solid curve shows a temperature profile calculated with the centerline as a reference point assuming the gas constant for air and the Gladstone-Dale constant in air. The speckle data show good consistency with the thermocouple data. The thermocouple data have not been attempted for any corrections for the radiation loss from the probe surface nor for the conduction heat loss through the probe stem. The probe corrections must know the emissivity of the probe surface, the time constant of the probe material, and the flow Reynolds number [14]. The present experiment allowed only a rough estimate of these values that would result in corrections with broad ranges. It is estimated that the temperature correction for the heat losses could upshift the thermocouple data as much as 20% near the flame center, which would enhance the agreement in the temperature comparison.

To explore an explanation for the discrepancy shown in the flat ambient region outside the flame, the effects of the constants R and K on the temperature profile evolution were examined. Strictly speaking, both the specific gas constant and the Gladstone-Dale constant must be estimated for the mixture of gases presented in the flame [15, 16]. As the

mass fractions of the product gases were not specifically known in the present experiment, only the extreme cases were examined as a guide for limiting conditions. Being a primary function of the light wave length with relatively weak dependence on the gas species, the Gladstone-Dale constant K for air is expected to be a fairly acceptable approximation for the propane flame. However, the gas constant R varies rather significantly for gas species. The dashed curve represents a temperature profile assuming a gas constant for 100% propane while keeping the Gladstone-Dale constant for air. The discrepancy in the ambient region has been diminished significantly in this limit, whereas the midrange temperature profile shows more deviations from the thermocouple data. Two corrections can reduce this increased discrepancies: (1) the thermocouple probe corrections would raise the thermocouple data to a noticeable degree, and (2) the corrections for the nonradial angular refraction would lower the specklegram temperature data.

CONCLUSION

The specklegram technique associated with Abel conversion is feasible as a new nonintrusive tool for flame temperature measurement diagnostics. Several points that contribute to the diagnostic improvements are

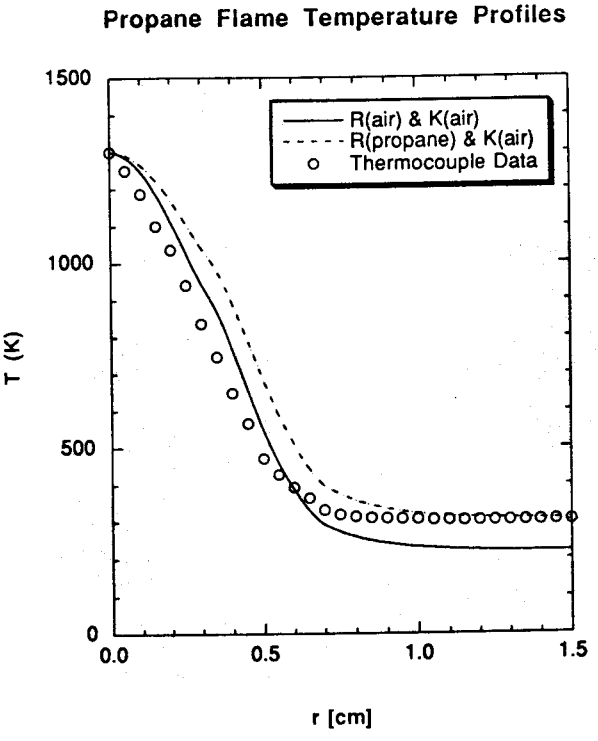

Fig. 8 Comparison of temperature profile obtained from deconvolved refractive index with thermocouple-measured temperature data for an axisymmetric propane Bunsen flame.

1. The correction for nonradial refraction and a modification of the paraxial assumption can significantly improve the data accuracy.
2. The correction for the thermocouple probe heat losses will provide a more accurate cross-calibration capabilities of the speckle photography technique.
3. The numerically stiff nature of the inverse Abel conversion integral might be avoided by devising a more stable algorithm such as a forward regression that requires neither a functional inversion nor numerical integration.

REFERENCES

1. D. Kastell, K. D. Kihm, and L. S. Fletcher, Study of Laminar Thermal Boundary Layers Occurring Around the Leading Edge of a Vertical Isothermal Wall Using a Specklegram Technique, *Exp. Fluids*, vol. 13, pp. 249–256, 1992.
2. A. C. Kak and M. Slaney, *Principles of Computerized Tomographic Imaging*, IEEE Press, New York, 1988.
3. G. T. Herman, *Image Reconstruction from Projections: Fundamentals of Computerized Tomography*, Academic Press, 1980.
4. S. R. Deans, *The Radon Transform and Some of Its Applications*, John Wiley, New York, 1983.
5. M. Françon, *Laser Speckle and Applications in Optics*, pp. 1–161, Academic Press, New York, 1979.
6. U. Wernekinck and W. Merzkirch, *Measurement of Natural Convection by Speckle Photography, Heat Transfer 1986*, C.L. Tien et al., ed., Hemisphere Publishing Corp., Washington, 1986.
7. K. D. Kihm and S. K. R. Cheeti, Study of Thermal Flows from Two-Dimensional, Upward-Facing Isothermal Surfaces Using a Laser Speckle Photography Technique, *Exp. Fluids*, vol. 17, pp. 246–252, 1994.
8. J. Z. Shu and J. Y. Li, A Laser Schlieren-Speckle Interferometry System for Measurement of Phase Objects, *J. Flow Visual. Image Process.*, vol. 1, pp. 63–68, 1993.
9. R. Rangayyan, A. P. Dhawan, and R. Gordon, Algorithms for Limited-View Computed Tomography: An Annotated Bibliography and a Challenge, *Appl. Optics*, vol. 24, no. 3, pp. 4000–4012, 1985.
10. R. Gordon, A Tutorial on ART, *IEEE Trans. Nucl. Sci.*, vol. NS-21, pp. 78–92, 1974.
11. M. Born and E. Wolf, *Principles of Optics*, pp. 128–130, Pergamon Press, Oxford, 1959.
12. K. D. Kihm, J. H. Kim, and L. S. Fletcher, Investigation of Natural Convection Heat Transfer in Converging Channel Flows Using a Specklegram Technique, *J. Heat Transfer*, vol. 115, pp. 140–148, 1993.
13. F. Vest, *Holographic Interferometry*, pp. 344–377, John Wiley, New York, 1979.
14. R. J. Moffat, The Gradient Approach to Thermocouple Circuitry, *Measure. Control Sci. Ind.*, vol. 3, part 2, pp. 33–37, 1962.
15. F. J. Weinberg, *Optics of Flames*, 1963.
16. W. C. Gardiner, Y. Hidaka, and T. Tanzawa, Refractivity of Combustion Gases, *Combust. Flame*, vol. 40, pp. 213–219, 1981.